applied sciences

MDPI

Article

Electrically Tunable Perfect Terahertz Absorber Using Embedded Combline Graphene Layer

Amir Maghoul [1,*], Ali Rostami [2], Azeez Abdullah Barzinjy [3,4] and Peyman Mirtaheri [5,*]

1 Department of Electronic Systems, Norwegian University of Science and Technology, 7491 Trondheim, Norway
2 Photonics and Nanocrystal Research Lab. (PRNL), Faculty of Electrical and Computer Engineering, University of Tabriz, Tabriz 5166614761, Iran; rostami@tabrizu.ac.ir
3 Department of Physics, College of Education, Salahaddin University, Erbil 44001, Kurdistan Region, Iraq; azeez.azeez@su.edu.krd
4 Physics Education Department, Faculty of Education, Tishk International University, Erbil 44001, Kurdistan Region, Iraq
5 Department of Mechanical, Electronics and Chemical Engineering, OsloMet—Oslo Metropolitan University, 0167 Oslo, Norway
* Correspondence: amir.maghoul@ntnu.no (A.M.); peyman.mirtaheri@oslomet.no (P.M.)

Abstract: Graphene is a powerful 2-D matter with the capability of extraordinary transparency, and tunable conductivity is employed in emerging optoelectronics devices. In this article, the design of an electrically tunable graphene-based perfect terahertz absorber is proposed and evaluated numerically. The introduced structure is composed of two graphene layers with a sharp absorption peak in the terahertz band. These graphene layers are combline and stripline separated by the insulator substrate. The position of the absorption peak is tunable on the absorption band by means of manipulation in geometric parameters of the combline graphene layer. Furthermore, the intensity and frequency of the absorption peak can be flexibly modulated by varying Fermi potential of the combline graphene layer, which can be controlled through external DC voltages without the need of changing the geometry of the structure. It is shown that the absorption band can be tuned in the bandwidth from 5 to 15 in terahertz. The findings of this paper can promote a new perspective in designing perfect ribbon absorbers based on graphene properties that can be utilized for future photodetectors, solar cells, and thermal sensors with an absorption intensity above 2×10^5 (nm^2) with narrow absorption bandwidth of 0.112 THz.

Keywords: graphene; perfect absorber; plasmon; fermi energy; tunable

Citation: Maghoul, A.; Rostami, A.; Barzinjy, A.A.; Mirtaheri, P. Electrically Tunable Perfect Terahertz Absorber Using Embedded Combline Graphene Layer. *Appl. Sci.* **2021**, *11*, 10961. https://doi.org/10.3390/app112210961

Academic Editor: Nuno Silva

Received: 15 October 2021
Accepted: 17 November 2021
Published: 19 November 2021

1. Introduction

In recent years, terahertz electronic devices have been significantly developed by utilizing metamaterials properties, and many researchers are attracted to this field. Working on the metamaterial regime due to exotic features with an exceptional conductivity leads to the creation of great high-tech achievements [1,2]. With the advent of the Surface Plasmon Resonance(SPR) phenomenon, the fabrication procedure of equipment based on terahertz technology is also revolutionized, especially manufacturing detectors and perfect absorbers [3,4]. The various wide range of absorbers as polarization insensitive/dependent absorbers [5,6], broad/narrowband absorbers [7–9], hyperbolic absorbers [10], plasmonic absorber [11,12], and van der Waals (vdW) absorbers [13,14] have been engineered from microwave [15], through terahertz [16], infrared [17], and also into the visible range [18]. Recently, perfect absorbers composed of graphene have demonstrated a satisfactory performance due to its extraordinary electrical properties, optical transparency, flexibility, high electric mobility, and controllable conductivity [19].

Graphene is a 2D nanomaterial comprising one monolayer of carbon atoms organized in a honeycomb lattice [20,21]. Within infrared and terahertz frequency range, the surface

plasmon polariton properties of graphene make this potential to generate the sharp peaks in the broad spectral region undertaking interaction between the incident light and graphene configuration, which can design such as nanostripes, nanoribbons, nanodisks, rings, and L-shaped arrays [22]. On one aspect, the conductivity surface of graphene plays a crucial role in setting the plasmonic resonance in the absorption band. The electrostatic control of conductivity gives the potential to adjust peaks regarding plasmonic resonances in perfect absorbers and detectors constructed by graphene [23–25]. Graphene can function as a gate-voltage element whose optical features depend on chemical potentials that can be varied using an external voltage. On this basis, the optical response in the absorption band can be engineered through structures that are configured with graphene [26]. Recent studies illustrate a particular attraction in the design of absorbing devices based on a single graphene layer and investigations of design challenges in the near-infrared and visible ranges [27,28]. For microwave range, the graphene layer is also interestingly used to design an optically tunable absorber [29] and switchable radar absorbing surfaces [30]. One of the most straightforward configurations that can be utilized to design a tunable terahertz absorber is combline architecture. Such structures have already been used to design radiofrequency filters for wireless and mobile applications based on advantages as small size, low cost of its fabrication, and high-quality factor [31,32].

This article proposes a unique absorber structure composed of graphene combline layers and a stripline with a particular metal and insulator configuration, which can be tuned independently by an external voltage bias. The results regarding the suggested structure are established via highly numerical simulations in CST Microwave Studio. Shifting the resonant peak of the presented absorber is demonstrated by applying voltage bias as the Fermi level of graphene changes. Moreover, the effect of the size variation of the graphene layers on the current configuration is evaluated. The electric field distribution on the conductivity surface of graphene is to be revealed by finding a better understanding of the involved physical mechanisms.

2. Theoretical Background

The conductivity surface plays a major role in creating the resonant peak through the absorption band for graphene-based absorbers. Graphene's conductivity surface is expressed by Kubo formula [33], where interband and intraband contributions are as follows:

$$\sigma\left(\omega, E_f, \Gamma, T\right) = \sigma_{int\ er} + \sigma_{int\ ra}, \tag{1}$$

$$\sigma_{int\ ra} = \frac{2k_B T e^2}{\pi\hbar^2} \ln\left(2cosh\frac{E_f}{2k_B T}\right)\frac{i}{(\omega + i\Gamma)} = \frac{\alpha}{-i\omega + \Gamma} \tag{2}$$

$$\sigma_{int\ er} = \frac{e^2}{4\hbar}\left[H\left(\frac{\omega}{2}\right) + i\frac{4\omega}{\pi}\int_0^\infty \frac{H(\Omega) - H\left(\frac{\omega}{2}\right)}{\omega^2 - 4\Omega^2} d\Omega\right], \tag{3}$$

and,

$$H(\Omega) = \frac{sinh\left(\frac{\hbar\Omega}{k_B T}\right)}{\left[cosh\left(\frac{\hbar\Omega}{k_B T}\right) + cosh\left(\frac{E_f}{k_B T}\right)\right]} \tag{4}$$

where ω is the angular frequency, E_f describes graphene's Fermi energy, T is the temperature, K_B and e is Boltzmann constant and elementary charge respectively, and $\hbar$ also depicts the reduced Plank's constant. It has been proved, when the Fermi energy becomes bigger than photon energy($\hbar\omega/2$), the interband part of Equation (1) can be ignored in comparison with the amount of intraband part of the equation due to Pauli blocking [34]. Also, the conductivity of graphene can be described by selecting the intraband contribution of the

Drude model, as presented in Equation (2). On this basis, the plasma frequency of graphene is obtained as below that t_g is graphene layer's thickness in the structure:

$$\omega_p = \left[\frac{2e^2 k_B T}{\pi\hbar^2 \varepsilon_0 t_g} \ln\left(2cosh\frac{E_f}{2k_B T}\right)\right]^{1/2} = \sqrt{\frac{\alpha}{\varepsilon_0 t_g}} \quad (5)$$

On the other hand, the stimulation of graphene through external voltage bias and then changing Fermi level counts as one of the popular features for graphene. It has been established that if a DC bias voltage is applied to the structure positioned between two graphene layers, the Fermi energy (chemical potential) can be tuned. Therefore, the conductivity surface is adjustable. The approximated formula to estimate the relationship between bias voltage and Fermi energy level (chemical potential), is given as follows [35,36]:

$$\left|E_f\right| = \hbar v_f \sqrt{\frac{\pi\varepsilon_r \varepsilon_0 V_{DC}}{e t_s}} \quad (6)$$

Here, ε_r and ε_0 are the primitivity of spacer and vacuum, respectively. t_s also define spacer's thickness, and V_{DC} shows the external bias voltage. Furthermore, v_f is the Fermi velocity that is equivalent to 1.1×10^6 (m/s). The Fermi level can be set over a broad range between -1 eV to 1 eV. As an example, a Fermi level is tunned between 0.2 eV to 0.6 eV by applying DC voltages between -240 V to 240 V, correspondingly. For these kinds of absorbers with the spacer between the graphene layer to avoid dielectric breakdown, silicon dioxide (SiO_2) and Kapton are also suggested as appropriate insulators because of high dielectric breakdown and low voltage bias.

3. System Design

The schematic demonstration and geometric parameters of the designed model are illustrated in Figure 1. Three cube structures are stacked on each other, and from the top of the configuration, there is an insulator with a thickness of 50 nm (h1) and permittivity of 1.96 [22,37]. Beneath it, another insulator with a depth of 1.5 µm (h2) with identical permittivity has been placed. In the third layer, a structure of gold with a thickness of 3 µm (h3) is positioned, which functions as a mirror substrate for THz waves. Two additional layers of graphene were added to the structure. One of these layers is located above the insulator and has a nano-stripline, while the other one is embedded between the first and the second insulator one and has a comb design. The combline patch on the intermediate substrate is initially dimensioned according to Table 1. The length and width of the square shape of the cell unit are equivalent to 400 nm. In simulations, the Drude model is also employed for the gold substrate. On this model, the permittivity of bulk gold is determined via $\varepsilon_\infty = 1$, the plasma frequency $\omega_p = 1.37 \times 10^{16}$ s^{-1} and damping constant $\omega_r = 1.23 \times 10^{14}$ s^{-1} [27].

In the case of the graphene layer, the conductive surface has opted for analysis of construction, and the graphene layer's thickness is 1nm in the model [38,39]. For extraction of the desired conductivity concerning graphene by Equation (2), we consider the temperature and relaxation time as 300 K and 1 ps, respectively [28,40]. Considering the appropriate data related to temperature and relaxation time is essential for the structure design because these parameters can change the conductivity and optical properties of the graphene sheet. As mentioned earlier, the initial geometric values of the combline graphene layer are demonstrated in Table 1. Accordingly, the number of ribbons of the graphene layer in the initial design is 23 on each side.

Table 1. Initial geometries of the combline graphene layer embedded for perfect absorber.

Parameter	p (nm)	s (nm)	d (nm)	t (nm)	G (nm)	L (nm)	W (nm)
Size value	7.5	10	25	6.25	25	400	400

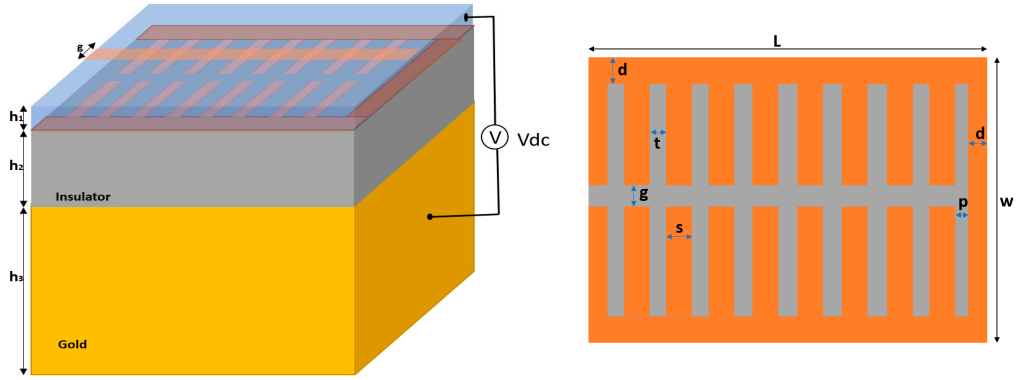

(**a**) (**b**)

Figure 1. Schematic diagram of terahertz graphene absorber. (**a**) 3D structure. (**b**) From the top view.

In order to evaluate the proposed structures in terms of functionality, the absorption cross-section (ACS) parameter as a measure of the absorption process is obtained, and its relationship with the absorption efficiency is defined by [41]:

$$Q_{abs} = \sigma_{abs}/A \tag{7}$$

Where σ_{abs}, Q_{abs} and A are the absorption cross-section (ACS) normalized, absorption efficiency, and cross-sectional area, and the absorption efficiency corresponds to the cross-section normalized to the geometrical area of the structure. The simulations are carried out by numerical computations based on finite integration technique (FIT) in CST Microwave Studios. We employ a time domain solver of CAD to extract the spectral response of the introduced perfect absorber in the absorption band. Further, the graphene used in the proposed combline structure is defined as a thin layer, and boundary conditions are considered open and space in different directions of the CAD environment around the implemented configuration. We utilize the default option of CAD in the meshing process of the simulation structure.

4. Simulation Results

First, the proposed absorber is implemented via the dimensions as mentioned above. A plane wave as an incident wave with the intensity of 1 $^{v}/_{m}$ shines to structure from the top, whereas the incidence vector is aligned with the normal vector of the combline conductive surface of graphene. The transmission parameter concerning the proposed structure is negligible due to the thickness of the gold substrate and its high refractive properties; hence absorption and reflection factors count as the key parameters to affect the optical characterizations of configuration. In addition, the initial Fermi energies considered for graphene layers are E_f = 0.43 eV for the nanostripe line, E_f = 0.7 eV for combline configuration. These Fermi levels can be provided by applying DC bias voltage separately to each graphene layer available in the absorber configuration. Based on the initial geometry of the modeled absorber, Absorption Cross-Section (ACS) of the structure is computed numerically in the considered absorption band, as demonstrated in Figure 2. The simulated result shows that the proposed absorber's absorption peak happens on 11.348 THz in the absorption band with an absorption rate of 2.366 $\times$ 10^5 nm^2. Electromagnetic field distributions of the developed model for transverse electric (TE) and transverse magnetic (TM) modes in absorption peak indicate that the combline graphene layer of the model plays

the leading role in the creation of an absorption peak and stimulate plasmon polaritons, and the coupling effect on the nano stripline is trivial, as shown in Figure 3. This means that electron density on the nano stripline in this state is minor due to the small width of the graphene stripline. In the following, this can be outlined that manipulating the Fermi level in the combline layer can shift absorption peak in the spectral characterization, and TE mode plays a predominant role in the radiation profile of the proposed structure. In detail, the electron concentration over the combline sheet embedded between two insulators under interaction with incident light provides a powerful plasmonic scattering that maximum value of the electric field can be seen in the gap between combline's ribbons. As a theoretical point, TE and TM modes are introduced as indicators for polarization inside a device in which only electric field for TE mode and magnetic field only for TM mode are considered along the direction of propagation.

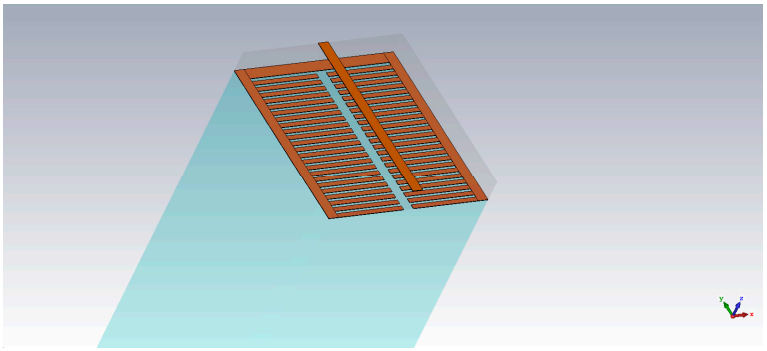

(**a**)

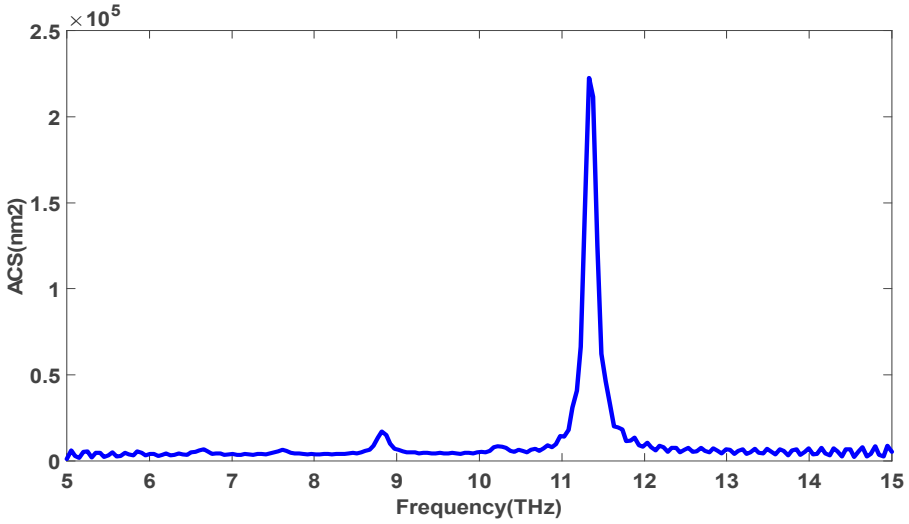

(**b**)

Figure 2. (**a**) the implemented configuration of THz combline perfect absorber, (**b**) Absorption Cross Section (ACS) of the proposed absorber.

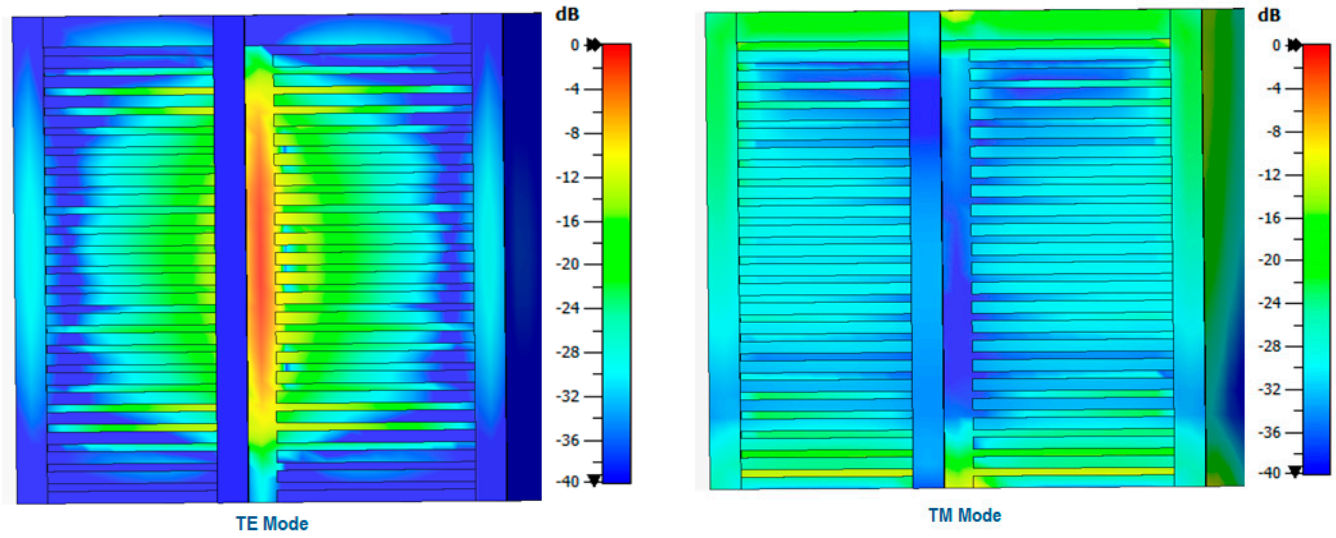

Figure 3. Electromagnetic field distribution for TE and TM modes in the peak of absorption.

To explore the concept with the change effect of geometric specifications of the combline graphene layer on spectral characterization of the absorber is investigated by focusing on the size and number of nanoribbons and the distance between them from each other. In the first step, the ribbon width of the combline graphene layer is manipulated. On this basis, the variation of the initial parameters of the ribbon layer is categorized as Table 2. It is clear that absorption characteristics of the proposed absorber change under the impact of size variation of combline graphene layer because the surface plasmon on this layer has a decisive role in determining absorbance rate. With this in coordination, simulation results in Figure 4a also indicate variations of absorption parameters as depicted earlier. Table 3 shows the changes in absorption parameter numerically.

Table 2. Manipulation of size parameters on the combline graphene layer.

Geometric Specification	s (nm)	t (nm)	p (nm)
Variation.I	8	8.25	9.5
Variation.II	12	4.5	7.5
Variation.III	6	10.25	11.5

In the continuation of this work, the width of the upper layer of graphene is changed from 25 nm to 5 nm, 65 nm, 100 nm, 140 nm to evaluate the impact of the graphene stripline existence on the absorption peak. The electric field distribution of structure in Figure 3 indicates the weak couplings of stripline; however, widening the stripline can influence the absorption characterization by providing a good scattering effective area and altering the scattering profile of the structure. In other words, an increase in nano-stripline width leads to creating a broader surface with the potential for more electron concentration; consequently, interaction incident light with graphene stripline manipulates localized surface plasmon of graphene, which shifts plasmonic resonance upon absorption band. In addition, an enhancing trend happens, which is due to increased electron density. Figure 4b and Table 4 demonstrate the simulation results related to the manipulations as mentioned above.

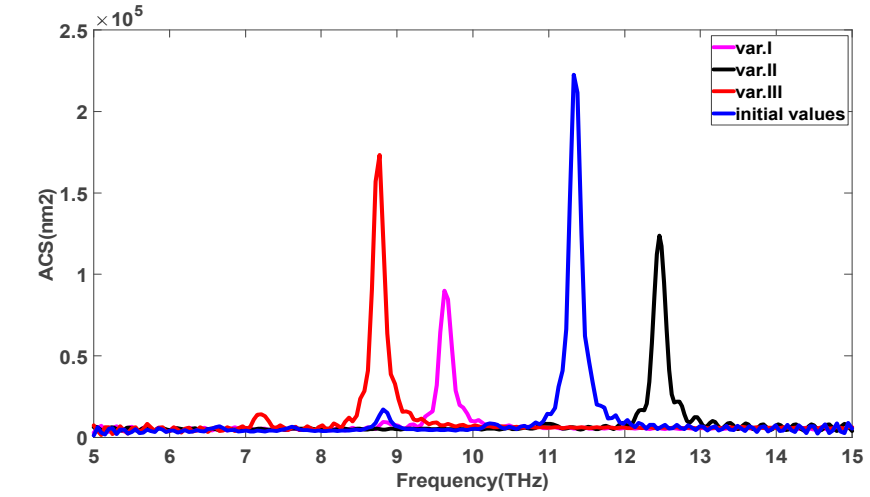

(**a**)

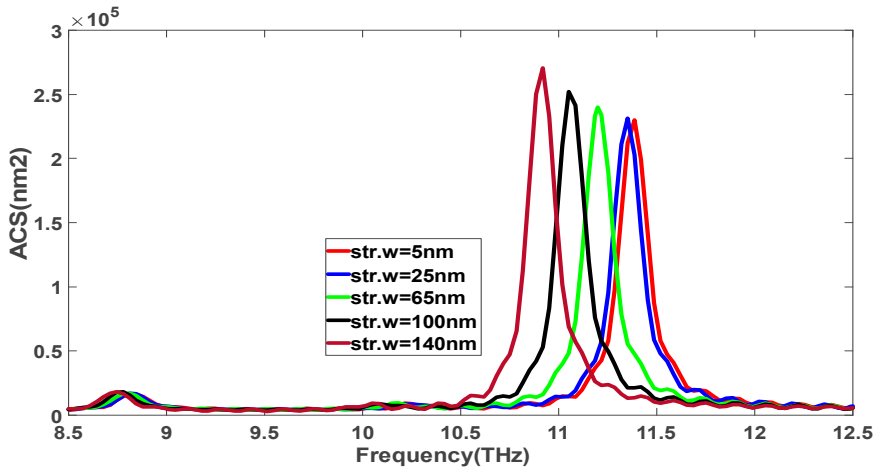

(**b**)

Figure 4. (**a**)The influence of geometric variation of ribbons on ACS of the perfect absorber, (**b**) the effect of changing in the width of graphene stripline layer on ACS of the absorber.

Table 3. Variations of absorption characteristics due to size manipulations.

Geometric Specification	Plasmonic Resonant Frequency (THz)	Absorption Intensity ($\times 10^5$ nm^2)
Initial size	11.348	2.366
Variation I	8.77	1.732
Variation II	9.622	0.9014
Variation III	12.456	1.24

Table 4. Variations of absorption characteristics due to stripline's width manipulations.

The Width of Graphene Stripline (nm)	Plasmonic Resonant Frequency (THz)	Absorption Intensity ($\times 10^5$ nm^2)
5	11.386	2.299
25	11.346	2.366
65	11.2	2.4
100	11.052	2.521
140	10.92	2.704

In general, it can be understood from the results in Figure 4a,b, and Tables 3 and 4, the resonant frequency and absorption peak on the spectral response of the structure are shifted by changing the size of ribbons. In further detail, manipulating the ribbon area causes the effective permittivity of configuration to vary due to change in effective area for electron concentstion [42,43]. Thus, the plasmon mode of the structure changes, and a new electromagnetic field profile is generated. Accordingly, the proposed model's absorption amplitude and resonant frequency are altered in each term of variations; that is why absorption intensity goes up and down due to the constructive and destructive effects of the scattering profile. The impact of stripline width (str.w) change on the absorption spectrum appears a redshift on the absorption band. An increase in absorption amplitude in both size variations because of enlarging the effective conductive area was observed.

Then, we focus on the number of available teeth of the combline graphene layer, considering 23 on each side of the initial design. To understand the effect of combline's teeth, the number of ribbons is first decreased to 17 on each side while the dimensions of the ribbons are fixed (s = 10 nm). In this state, the initial geometries of the combline configuration are turned into t = 12.25 nm and p = 9 nm. The simulated results in Figure 5 and Table 5 demonstrate, a redshift happens on the absorption band. Also, the absorption amplitude experiences a lower intensity rather than the absorption value of the initial architecture. Next, the teeth number of the graphene layer of the configuration is increased to 26 ribbons on each side. On this basis, the original specifications of the graphene layer are converted to t = 4.25 nm, p = 8.75 nm. An increase in the number of ribbon teeth enhances the absorption amplitude in addition to blueshift. It is mainly because more surfaces of the combline graphene layer are subjected to the incident wave that means more electron density on the graphene surfaces, and absorption intensity is enhanced. Also, shifting absorption peak over frequency is due to altering the surface plasmons in size manipulation. As a notable point, it is worth mentioning that the ribbons play a determining role in the frequency assignment of plasmonic modes over the absorption band and function as a frequency selective surface (FSS). In addition, a nano strip on the top of the insulator can present a tunability potential for plasmonic resonance due to coupling that directly affects the plasma frequency.

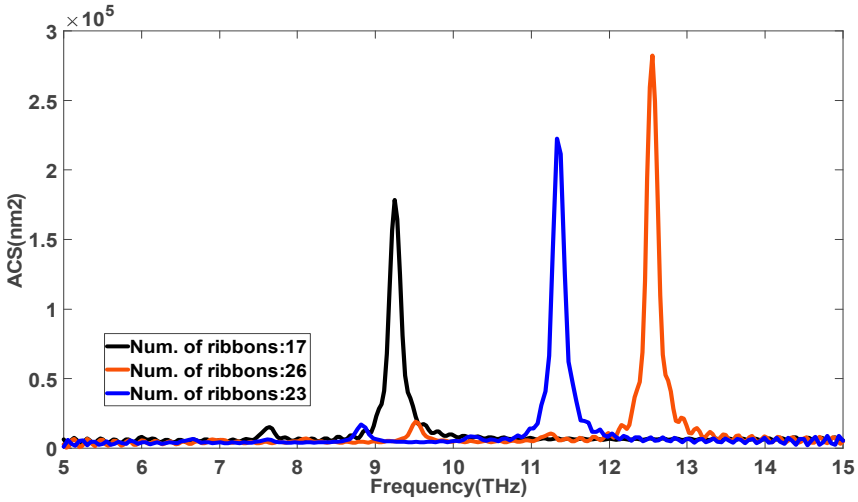

Figure 5. The influence of designed ribbons number of the graphene layer on ACS of perfect absorber.

Table 5. Variations of absorption characteristics under change of teeth number of combline structure.

The Number of Ribbon Teeth	Plasmonic Resonant Frequency (THz)	Absorption Intensity ($\times 10^5$ nm^2)
N = 17	9.246	1.784
N = 23	11.346	2.366
N = 26	12.556	2.823

For more study, the size influence of the g-distance of the designed configuration on the absorbance factor is assessed. In this regard, the g parameter is scaled to 10 nm, 20 nm, 30 nm, 40 nm, 50 nm while the stripline width is fixed at 25 nm, and then the corresponding absorption characteristic is simulated numerically. As shown in Figure 6 and Table 6, it is well-recognized that g-distance can adjust the amplitude and frequency of absorption on the spectral response of the designed perfect absorber. By size increase in the gap of g, the activated combline surface of the graphene layer becomes smaller, which means dropping in absorption intensity. Moreover, a blueshift is detected over the spectra presented in Figure 6. As an overall result, manipulating the developed model's geometric specification allows the perfect absorber's plasmon peak position and absorption amplitude to be tunned on the absorption band.

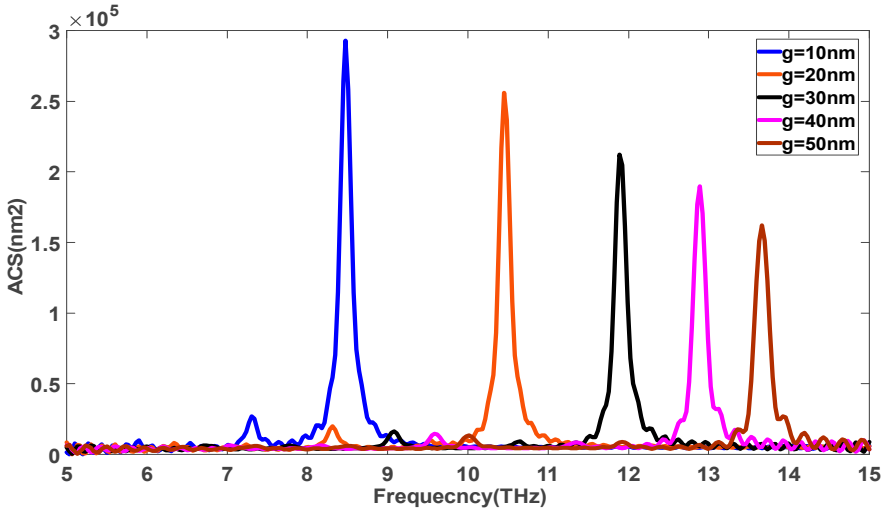

Figure 6. The influence of g variations on ACS of proposed perfect absorber.

Table 6. Variations of absorption characteristics under change of the distance two ribbons in two sides of the structure (g-distance).

g-Distance (nm)	Plasmonic Resonant Frequency (THz)	Absorption Intensity ($\times 10^5$ nm^2)
10	8.477	2.929
20	10.45	2.56
25	11.348	2.366
30	11.89	2.122
40	12.891	1.899
50	13.66	1.822

Outstandingly, one of the unique properties of graphene layers is that they can be controlled via Fermi energies change. As previously mentioned, the Fermi levels of graphene layers can be tunned by an external DC source. In the developed structure, two layers of graphene with different Fermi levels, including E_f = 0.7 eV for combline layer and E_f = 0.43 eV for nano stripline are embedded. Since the coupling effect of the upper graphene layer in interaction with light was negligible due to its small width in the initial

structure. The results from Figure 3 show that the combline graphene layer was introduced as an active surface for the stimulation of plasmon modes; thus, we are intended to evaluate the impact of Fermi potential change on the absorbance rate of the model in the absorption band. It is important to note that wider graphene stripline exhibits an influential role, and changes in its Fermi level alter the absorption response.

Nevertheless, the Fermi potential of the combline graphene layer is tuned between 0.4 eV and 0.9 eV. Interestingly, the simulation results indicate that the resonant peak of the absorber linearly follows an increasing trend on the absorption spectrum, and a blue shift occurs, as shown in Figure 7. Also, the absorption intensity of the designed absorber is regularly enhanced with the increase in Fermi energy. In other words, the absorption spectra of structure move upon the absorption band by adjusting Fermi potential without manipulating absorber geometries.

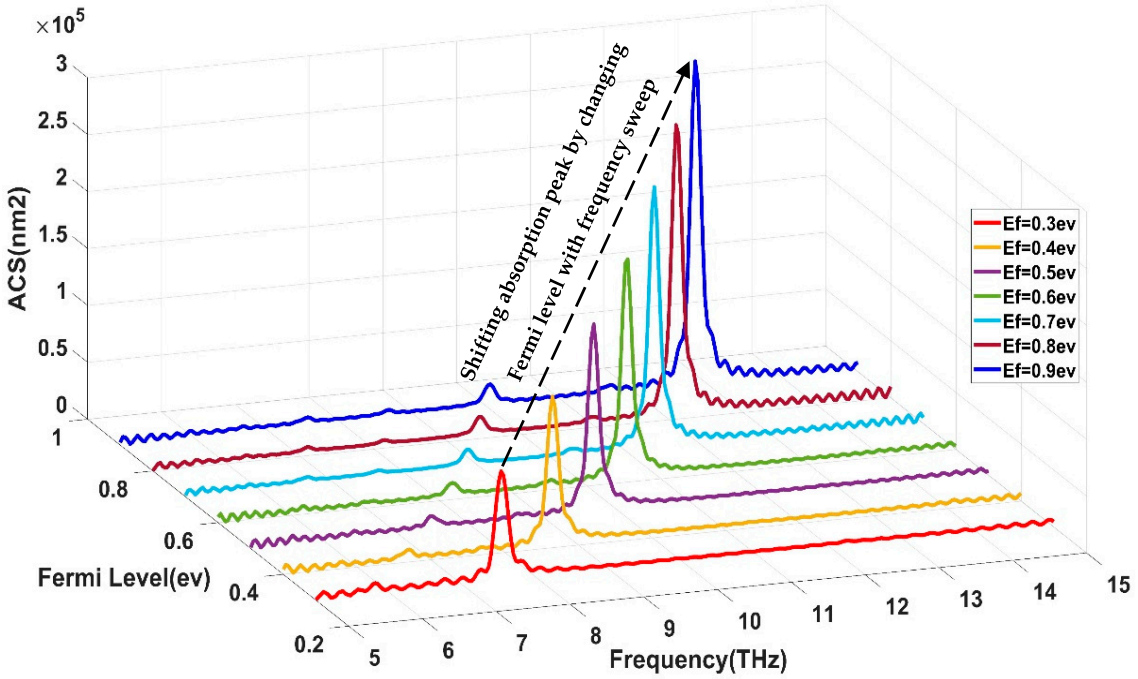

Figure 7. Spectral sweep of the modeled perfect absorber by Fermi level changing.

Given that the Fermi level is adjustable with external DC voltages, it can be a practical procedure to manufacture a tunable combline graphene perfect absorber based on the presented design. Blueshift and enhancement of absorption intensity are well highlighted in Figure 7 and Table 7 when the Fermi potential of the combline graphene layer changes. In detail, the Fermi level lies in the forbidden gap between the valence and conduction bands from the electronic physics point of view. Therefore, increasing the Fermi energy leads the electrons from the valance band to move to the conduction band. In this state, the Fermi potential increases and becomes close to the conduction band in terms of energy levels and electron density increases, resulting in a plasmonic modes shift [44].

Table 7. The variation of absorption parameters under changisng in combline' Fermi potential.

Fermi Potential (eV)	0.4	0.5	0.6	0.7	0.8	0.9
Plasmonic resonant frequency(THz)	8.644	9.647	10.55	11.353	12.09	12.79
Amplitude of absorption peak($\times 10^5$ nm^2)	1.3285	1.671	1.959	2.314	2.584	2.871

The most important advantage of the proposed combline absorber can be mentioned to the ease of practical implementation and simplicity of fabrication. The designed structure has the potential for simple structure fabrication, high absorption efficiency, and stability, with a bandwidth around 112 GHz, and small size. For the implementation of the proposed structures, it is clear that the standard microelectronic fabrication planar method can be used. Optical lithography at a submicron level and electron beam lithography at a nanoscale or deep submicron level can be used to image the combline layer in the proposed perfect absorber [45]. In further detail, first, an appropriate insulator is prepared, and then a graphene sheet can be implemented by large-scale transfer techniques, and so the photoresist is spin-coated on the graphene sheet. After doing the standard steps in photolithography, a mask is prepared for the combline layer, and then, by photoimaging, the pattern is shaped on the resist. After removing the resist on the graphene layer and developing a suitable solvent, the combline graphene pattern appears on the top of the substrate. Based on the available technologies of Electron Beam lithography(EBL), there is the potential for size miniaturization to reduce down about 5 nm [46]. The proposed perfect absorber can be introduced as a pioneering candidate in terms of application like a refractive index sensor, thermal emission sensor, or a nanosensor to detect bacterial and viral particles.

5. Conclusions

In summary, we have proposed a new design of the solid tunable absorber comprising of an embedded combline graphene layer and a nano stripline that an insulator inserted between them. The results reveal, by changing the geometrical parameters of ribbons in the combline graphene layer, redshift and blueshift happen that lead to shifting absorption peak on the spectral response of the absorber, and absorption intensity is also altered. A unique feature of our developed perfect absorber is that its absorption peak had the flexible potential to tune on the absorption band by adjusting the Fermi level of the combline layer of graphene instead of refabrication and manipulation of absorber's geometries. In other words, the desired absorption peak can be attained by setting a specific Fermi level that correlates with external DC voltage, as described in our model. We highlighted shifting absorption peak using variations of Fermi level on a 3D diagram similar to the frequency sweep. These results imply that the designed simple perfect absorber based on the combline graphene layer can be an applicable candidate for a wide range of photonic devices and sensory equipment.

Author Contributions: A.M. designed the structures and simulations and wrote the paper. A.R. designed the concept, supervised the work, edited the paper, and reviewed it, A.A.B. read the paper and revised it. P.M. supervised the work, technically investigated, and completed editing, and reviewed and funded it. All authors have read and agreed to the published version of the manuscript.

Funding: This work was supported by the Optical/NIFR Lab of the Department of Mechanical, Electronics and Chemical Engineering(MEC), OsloMet—Oslo Metropolitan University.

Institutional Review Board Statement: Not applicable.

Informed Consent Statement: Not applicable.

Data Availability Statement: Not applicable.

Conflicts of Interest: The authors declare no conflict of interest.

References

1. Banerjee, S.; Pal, B.P.; Roy Chowdhury, D. Resonance phenomena in electromagnetic metamaterials for the terahertz domain: A review. *J. Electromagn. Waves Appl.* **2020**, *34*, 1314–1337. [CrossRef]
2. Xu, W.; Xie, L.; Ying, Y. Mechanisms and applications of terahertz metamaterial sensing: A review. *Nanoscale* **2017**, *9*, 13864–13878. [CrossRef]
3. Nejat, M.; Nozhat, N. Sensing and switching capabilities of a tunable GST-based perfect absorber in near-infrared region. *J. Phys. D Appl. Phys.* **2020**, *53*, 245105. [CrossRef]

4. Yi, Z.; Liang, C.; Chen, X.; Zhou, Z.; Tang, Y.; Ye, X.; Yi, Y.; Wang, J.; Wu, P. Dual-band plasmonic perfect absorber based on graphene metamaterials for refractive index sensing application. *Micromachines* **2019**, *10*, 443. [CrossRef]
5. Grant, J.; Ma, Y.; Saha, S.; Khalid, A.; Cumming, D.R.S. Polarization insensitive, broadband terahertz metamaterial absorber. *Opt. Lett.* **2011**, *36*, 3476–3478. [CrossRef]
6. Mao, Z.; Liu, S.; Bian, B.; Wang, B.; Ma, B.; Chen, L.; Xu, J. Multi-band polarization-insensitive metamaterial absorber based on Chinese ancient coin-shaped structures. *J. Appl. Phys.* **2014**, *115*, 204505. [CrossRef]
7. Qiu Xu, Y.; Heng Zhou, P.; Bin Zhang, H.; Chen, L.; Jiang Deng, L. A wide-angle planar metamaterial absorber based on split ring resonator coupling. *J. Appl. Phys.* **2011**, *110*, 044102. [CrossRef]
8. Zhao, J.; Yu, X.; Yang, X.; Th Tee, C.A.; Yuan, W.; Yu, Y. Polarization-independent and high-efficiency broadband optical absorber in visible light based on nanostructured germanium arrays. *Opt. Lett.* **2019**, *44*, 963–966. [CrossRef] [PubMed]
9. Liao, Y.-L.; Zhao, Y. Ultra-narrowband dielectric metamaterial absorber with ultra-sparse nanowire grids for sensing applications. *Sci. Rep.* **2020**, *10*, 1480. [CrossRef] [PubMed]
10. Lu, G.; Wu, F.; Zheng, M.; Chen, C.; Zhou, X.; Diao, C.; Liu, F.; Du, G.; Xue, C.; Jiang, H.; et al. Perfect optical absorbers in a wide range of incidence by photonic heterostructures containing layered hyperbolic metamaterials. *Opt. Express* **2019**, *27*, 5326–5336. [CrossRef] [PubMed]
11. Gao, H.; Zhou, D.; Cui, W.; Liu, Z.; Liu, Y.; Jing, Z.; Peng, W. Ultraviolet broadband plasmonic absorber with dual visible and near-infrared narrow bands. *J. Opt. Soc. Am. A* **2019**, *36*, 264–269. [CrossRef]
12. Nguyen, D.M.; Lee, D.; Rho, J. Control of light absorbance using plasmonic grating based perfect absorber at visible and near-infrared wavelengths. *Sci. Rep.* **2017**, *7*, 2611. [CrossRef]
13. Xu, L.; Peng, B.; Luo, X.; Zhai, X.; Wang, L. A broadband and polarization-insensitive perfect absorber based on a van der Waals material in the mid-infrared regime. *Results Phys.* **2019**, *15*, 102687. [CrossRef]
14. Wang, S.; Yu, H.; Zhang, H.; Wang, A.; Zhao, M.; Chen, Y.; Mei, L.; Wang, J. Broadband Few-Layer MoS2 Saturable Absorbers. *Adv. Mater.* **2014**, *26*, 3538–3544. [CrossRef] [PubMed]
15. Jang, T.; Youn, H.; Shin, Y.J.; Guo, L.J. Transparent and Flexible Polarization-Independent Microwave Broadband Absorber. *ACS Photonics* **2014**, *1*, 279–284. [CrossRef]
16. Zhang, Y.; Feng, Y.; Zhu, B.; Zhao, J.; Jiang, T. Graphene based tunable metamaterial absorber and polarization modulation in terahertz frequency. *Opt. Express* **2014**, *22*, 22743–22752. [CrossRef] [PubMed]
17. Liu, N.; Mesch, M.; Weiss, T.; Hentschel, M.; Giessen, H. Infrared Perfect Absorber and Its Application as Plasmonic Sensor. *Nano Lett.* **2010**, *10*, 2342–2348. [CrossRef]
18. Ghobadi, A.; Hajian, H.; Gokbayrak, M.; Dereshgi, S.A.; Toprak, A.; Butun, B.; Ozbay, E. Visible light nearly perfect absorber: An optimum unit cell arrangement for near absolute polarization insensitivity. *Opt. Express* **2017**, *25*, 27624–27634. [CrossRef]
19. Gu, M.; Xiao, B.; Xiao, S. Tunable THz perfect absorber with two absorption peaks based on graphene microribbons. *Micro Nano Lett.* **2018**, *13*, 631–635. [CrossRef]
20. Novoselov, K.S.; Geim, A.K.; Morozov, S.V.; Jiang, D.; Zhang, Y.; Dubonos, S.V.; Grigorieva, I.V.; Firsov, A.A. Electric Field Effect in Atomically Thin Carbon Films. *Science* **2004**, *306*, 666–669. [CrossRef]
21. Geim, A.K.; Novoselov, K.S. The rise of graphene. *Nat. Mater.* **2007**, *6*, 183–191. [CrossRef] [PubMed]
22. Wu, D.; Wang, M.; Feng, H.; Xu, Z.; Liu, Y.; Xia, F.; Zhang, K.; Kong, W.; Dong, L.; Yun, M. Independently tunable perfect absorber based on the plasmonic properties in double-layer graphene. *Carbon* **2019**, *155*, 618–623. [CrossRef]
23. Lee, S.H.; Choi, M.; Kim, T.-T.; Lee, S.; Liu, M.; Yin, X.; Choi, H.K.; Lee, S.S.; Choi, C.-G.; Choi, S.-Y.; et al. Switching terahertz waves with gate-controlled active graphene metamaterials. *Nat. Mater.* **2012**, *11*, 936–941. [CrossRef]
24. Valmorra, F.; Scalari, G.; Maissen, C.; Fu, W.; Schönenberger, C.; Choi, J.W.; Park, H.G.; Beck, M.; Faist, J. Low-Bias Active Control of Terahertz Waves by Coupling Large-Area CVD Graphene to a Terahertz Metamaterial. *Nano Lett.* **2013**, *13*, 3193–3198. [CrossRef] [PubMed]
25. Yao, Y.; Shankar, R.; Kats, M.A.; Song, Y.; Kong, J.; Loncar, M.; Capasso, F. Electrically Tunable Metasurface Perfect Absorbers for Ultrathin Mid-Infrared Optical Modulators. *Nano Lett.* **2014**, *14*, 6526–6532. [CrossRef] [PubMed]
26. Li, H.; Wang, L.; Zhai, X. Tunable graphene-based mid-infrared plasmonic wide-angle narrowband perfect absorber. *Sci. Rep.* **2016**, *6*, 36651. [CrossRef]
27. Piper, J.R.; Fan, S. Total Absorption in a Graphene Monolayer in the Optical Regime by Critical Coupling with a Photonic Crystal Guided Resonance. *ACS Photonics* **2014**, *1*, 347–353. [CrossRef]
28. Vorobev, A.S.; Bianco, G.V.; Bruno, G.; D'Orazio, A.; O'Faolain, L.; Grande, M. Tuning of Graphene-Based Optical Devices Operating in the Near-Infrared. *Appl. Sci.* **2021**, *11*, 8367. [CrossRef]
29. Grande, M.; Bianco, G.V.; Perna, F.M.; Capriati, V.; Capezzuto, P.; Scalora, M.; Bruno, G.; D'Orazio, A. Reconfigurable and optically transparent microwave absorbers based on deep eutectic solvent-gated graphene. *Sci. Rep.* **2019**, *9*, 5463. [CrossRef]
30. Balci, O.; Polat, E.O.; Kakenov, N.; Kocabas, C. Graphene-enabled electrically switchable radar-absorbing surfaces. *Nat. Commun.* **2015**, *6*, 6628. [CrossRef]
31. Yao, H.; Wang, C.; Zaki, K.A. Effects of tuning structures on combline filters. In Proceedings of the 1996 26th European Microwave Conference, Prague, Czech Republic, 6–13 September 1996; pp. 427–430.
32. Awai, I. Design of Multistage Combline Band-Pass Filters in Layered Structures. In *Novel Technologies for Microwave and Millimeter—Wave Applications*; Kiang, J.-F., Ed.; Springer: Boston, MA, USA, 2004; pp. 83–100.

33. Andryieuski, A.; Lavrinenko, A.V. Graphene metamaterials based tunable terahertz absorber: Effective surface conductivity approach. *Opt. Express* **2013**, *21*, 9144–9155. [CrossRef]
34. Yao, Y.; Kats, M.A.; Genevet, P.; Yu, N.; Song, Y.; Kong, J.; Capasso, F. Broad Electrical Tuning of Graphene-Loaded Plasmonic Antennas. *Nano Lett.* **2013**, *13*, 1257–1264. [CrossRef] [PubMed]
35. Zhang, Y.; Li, T.; Chen, Q.; Zhang, H.; O'Hara, J.F.; Abele, E.; Taylor, A.J.; Chen, H.-T.; Azad, A.K. Independently tunable dual-band perfect absorber based on graphene at mid-infrared frequencies. *Sci. Rep.* **2015**, *5*, 18463. [CrossRef]
36. Gómez-Díaz, J.S.; Perruisseau-Carrier, J. Graphene-based plasmonic switches at near infrared frequencies. *Opt. Express* **2013**, *21*, 15490–15504. [CrossRef] [PubMed]
37. Zhang, J.; Zhu, Z.; Liu, W.; Yuan, X.; Qin, S. Towards photodetection with high efficiency and tunable spectral selectivity: Graphene plasmonics for light trapping and absorption engineering. *Nanoscale* **2015**, *7*, 13530–13536. [CrossRef]
38. Wang, X.; Shi, Y. CHAPTER 1 Fabrication Techniques of Graphene Nanostructures. In *Nanofabrication and Its Application in Renewable Energy*; The Royal Society of Chemistry: Cambridge, UK, 2014; pp. 1–30.
39. Nguyen, B.-S.; Lin, J.-F.; Perng, D.-C. 1-nm-thick graphene tri-layer as the ultimate copper diffusion barrier. *Appl. Phys. Lett.* **2014**, *104*, 082105. [CrossRef]
40. Dash, S.; Patnaik, A. Performance of Graphene Plasmonic Antenna in Comparison with Their Counterparts for Low-Terahertz Applications. *Plasmonics* **2018**, *13*, 2353–2360. [CrossRef]
41. Bohren, C.F.; Huffman, D.R. *Absorption and Scattering of Light by Small Particles*; John Wiley & Sons: Hoboken, NJ, USA, 2008.
42. Ullah, Z.; Witjaksono, G.; Nawi, I.; Tansu, N.; Irfan Khattak, M.; Junaid, M. A Review on the Development of Tunable Graphene Nanoantennas for Terahertz Optoelectronic and Plasmonic Applications. *Sensors* **2020**, *20*, 1401. [CrossRef] [PubMed]
43. Cen, C.; Chen, Z.; Xu, D.; Jiang, L.; Chen, X.; Yi, Z.; Wu, P.; Li, G.; Yi, Y. High Quality Factor, High Sensitivity Metamaterial Graphene—Perfect Absorber Based on Critical Coupling Theory and Impedance Matching. *Nanomaterials* **2020**, *10*, 95. [CrossRef] [PubMed]
44. Bott, A.W. Electrochemistry of semiconductors. *Curr. Sep.* **1998**, *17*, 87–92.
45. Stoliar, P.; Calò, A.; Valle, F.; Biscarini, F. Fabrication of Fractal Surfaces by Electron Beam Lithography. *IEEE Trans. Nanotechnol.* **2010**, *9*, 229–236. [CrossRef]
46. Nur, O.; Willander, M. (Eds.) Chapter 3—Conventional nanofabrication methods. In *Low Temperature Chemical Nanofabrication*; William Andrew Publishing: Norrköping, Sweden, 2020; pp. 49–86.